Landslides (2018) 15:1391–1400
DOI 10.1007/s10346-018-0985-1
Received: 8 December 2017
Accepted: 21 March 2018
Published online: 18 April 2018

Chaojun Ouyang · Wei Zhao · Qiang Xu · Dalei Peng · Weile Li · Dongpo Wang · Shu Zhou · Shunwei Hou

Failure mechanisms and characteristics of the 2016 catastrophic rockslide at Su village, Lishui, China

Abstract This paper describes a recent large rockslide, which occurred at Su village in Lishui, Zhejiang Province, China, on September 28, 2016. In the past decade, a vegetation-free deformed surface was clearly visible and frequent rockfalls were noticed. Due to strong sustained rainfall, approximately 0.4 million m^3 of granite blocks rapidly descended from the upper part of the hillside. The mass rushed into the V-shaped valley resulting in the formation of a barrier dam and dammed lake. The catastrophic rockslide caused 27 deaths and more than 20 houses were destroyed. The evolutionary process before the rockslide is clearly captured by high-resolution remote sensing images and photos. Video of the rockslide and field investigations show entrainment of superficial material in the middle and lower parts of the slope.

Keywords Catastrophic rockslide · Su village · Remote sensing image · Entrainment · Barrier dam

Introduction

Rockslides are among the most dangerous and damaging landslide phenomena due to their high mobility and large extent, despite being relatively uncommon and occurring in mountainous areas (Hungr and Evans 2004; Evans 2006). In the past 10 years, several large catastrophic rockslides occurred in China (Hu et al. 2009; Zhen et al. 2012; Chen et al. 2011; Xing et al. 2014; Zhou et al. 2015; Huang et al. 2016; Fan et al. 2017; Ouyang et al. 2017b). The failure mechanism and dynamic characteristics of rockslides are key factors in predicting future rockslides (Guthrie et al. 2009; Xu et al. 2010; Wu et al. 2013; Coe et al. 2016; Ouyang et al. 2017b; Wang et al. 2017). Nevertheless, the associated mechanism and characteristics of rockslides and pertinent granular flow are complicated and still under considerable debate (Sosio et al. 2008; Zhou and Sun 2013; Cui et al. 2017). Rockslides commonly disintegrate into flowing masses of fragments due to collision during the slide (Xu et al. 2010). Rockslides impose a stronger impact and traction force on the ground relative to soil landslides. In rockslides, the basal entrainment effect and volume enlargement are more pronounced and likely to form a barrier dam (Hungr and Evans 2004; Iverson and Ouyang 2015; Ouyang et al. 2017a).

At 17:28 (GMT+8) on September 28, 2016, a catastrophic rockslide suddenly collapsed and rushed down toward the houses in Su village, Lishui, Zhejiang, China (E 119° 18′ 13″, N 28° 47′ 03″). The slide was more than 0.4 million m^3 in volume. The huge rockslide buried more than 20 houses, caused 27 deaths, and was one of the most devastating geohazards in the history of eastern China. Rockslides are common in this area and the site was listed for relocation by the Chinese government. Local residents were moved out due to the heavy rainfall before the rockslide occurred. Unfortunately, a number of the residents returned to their houses. The rockslide was captured on video by local residents and can be viewed at (http://www.iqiyi.com/w_19ruhoy7hp.html). Video of the rockslide is useful for understanding rockslide dynamic processes. Through detailed field investigation, we examine the specific characteristics of the rockslide in order to help reduce or prevent future hazards.

Regional geological and geomorphology setting

The rockslide occurred at Su village in the municipality of Suichang county, Lishui (Fig. 1). Su village is situated in the southwestern Zhejiang province, 290 km away from the capital city of Hangzhou. The landscape is composed of mountains with middle and lower altitude as well as hills. Generally, the elevation gradually decreases from southwest to northeast. The study area is composed of late Jurassic to Cretaceous volcanic and clastic rocks underlain by Paleozoic clastic and carbonate rocks (Fig. 2). The mountain is mainly composed of cretaceous ignimbrite, volcanic clastic rock, rhyolite, orthophyre, sandstone, and quaternary debris accumulation. The crushed rocks are mainly of fine-grained monzogranite. Two main NE-trending faults cut the study area, the Yuyao-Lishui fault and the Songyang-Pingyang fault (Fig. 2). Other faults in the area are secondary faults derived from the two main faults. The rocks in the study area are extruded by old tectonic movement. The secondary structures, such as structural joints and weathered fractures, are relatively well-developed.

The rockslide is located at the top of the mountain behind Su village (Fig. 3a). The elevation of the mountain peak is 871 m a.s.l., and the relative elevation difference between the peak and the village is 531 m. Pre- and post-event images can be viewed in Fig. 3a, b. The elevation variations before and after the slide, as well as the landslide zoning, are shown in Fig. 3c, d. After the slide, the slide mass was mainly composed of crushed rocks (Fig. 4). The rocks are fine-grained monzogranite. The mineral composition of the rockslide is shown in Table 1. Rock and soil samples were collected at three different locations (Fig. 3b. The slide mass is primarily composed of coarse sand and rock. The particle size distribution of three different samples is shown in Fig. 5. Thirteen drill holes after the slide were dug by the third geological group of Zhejiang province. The location of the drilling holes is shown in Fig. 3d. The drilling properties of different layers are listed in geologic profile maps in Fig. 8. The bedrock primarily consists of high- to medium-weathered fine-grained monzogranite. The body

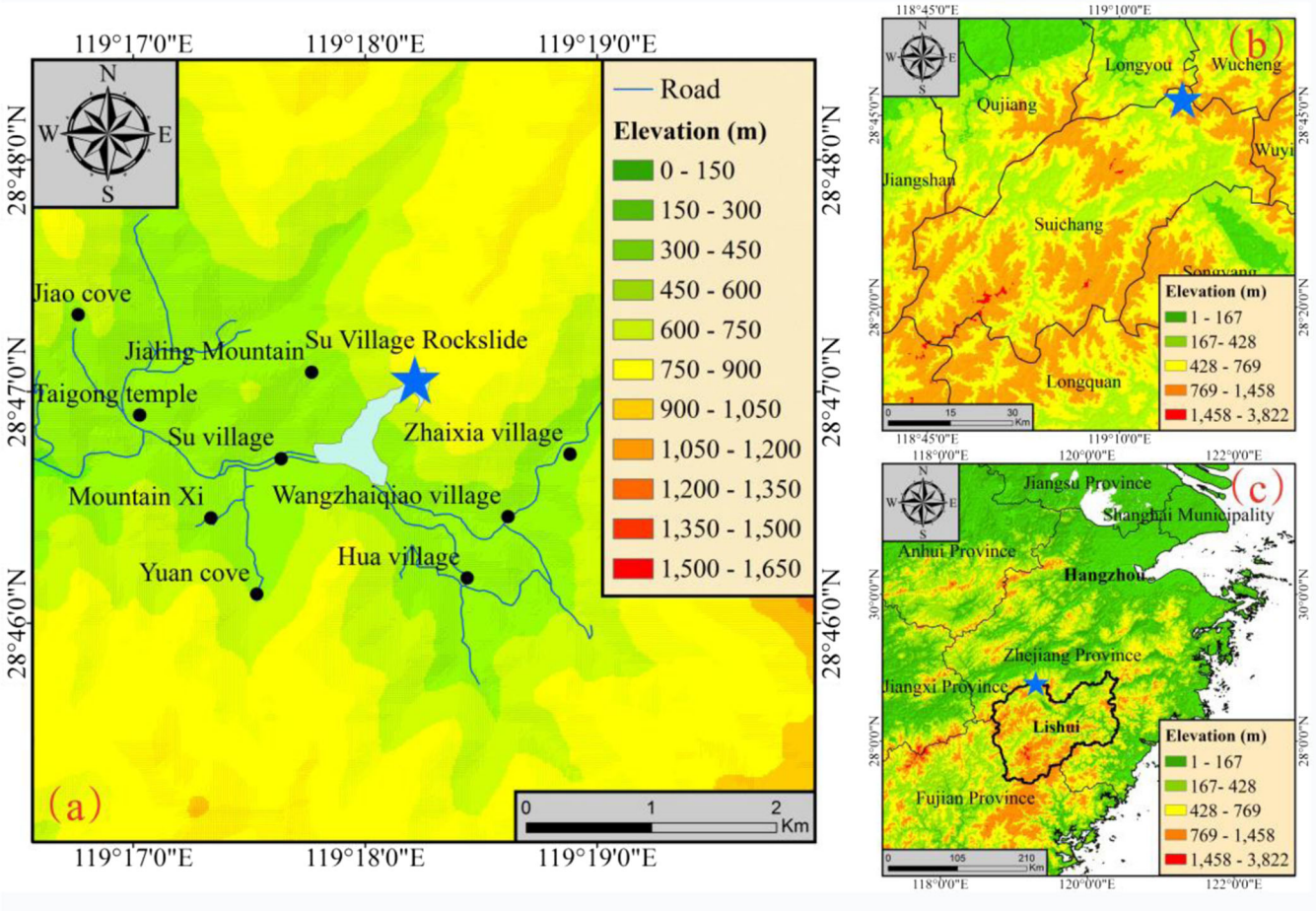

Fig. 1 Map showing the location of the **a** study area, **b** county, and **c** Zhejiang Province

of the rockslide in the source area is weathered granite, which gradually disintegrates during the slide.

The study area is largely covered by artificially planted bamboo. The study area has a middle subtropical monsoon climate with a mean annual temperature of 16.8 °C. Average monthly precipitation data of Lishui municipality is shown in Fig. 6a. The mean annual precipitation is 1407 mm. Approximately 80% of precipitation is concentrated between March and September. The precipitation 24 h before the slide was collected at the Wangzhaiqiao rainfall station, which is approximately 1 km away. Due to typhoon Catfish, the cumulative rainfall within 24 h of the slide at the Wangzhaiqiao rainfall station was 114.6 mm, as shown in Fig. 6b. It is almost close to the average value 124 mm in September. The sustained rainfall played a significant role in initiating failure of the rockslide.

Insights from remote sensing images and pre-disaster photos

In order to analyze the failure mechanisms of the rockslide, four high-resolution remote sensing images from KeyHole with 2 m precision from 2000 and Quickbird with 0.6 m precision in 2010, 2013, and 2015 and photos before the disaster are examined. As shown in Fig. 7a, obvious surface deformation is visible in the KeyHole images from 2000. Tensile fractures can be seen behind the rear of the rockslide. In addition, a naked collapsed surface without vegetation is visible, which is consistent with descriptions from villagers. One villager said there were frequent rockfalls within a short distance in the past decade. In 2010, a larger area of exposed rock surface became visible (Fig. 7b). From 2013 to 2015, the unstable zone continued to enlarge (Fig. 7c, d). An arcuate shape marked by red arrows in Fig. 7d formed. At this stage, the exposed surface is primarily located in the west portion of the source area. The area was classified as a high-risk area by local administrators. On September 27, one day before total failure, a more intense rockfall was noticed. The village was evacuated and most of the residents were moved to safe locations. Unfortunately, some people returned to their home as the rainfall stopped. Several photos before the rockslide were taken by local geologic surveyors. It is worth noting that a huge steep rock, which was close to vertical and marked by a dotted line in Fig. 7e, evolved fast. On September 13, more collapsed deposits accumulated on the west side of the steep rock. A new deep gully in the east part of the rock also formed. From the side view in Fig. 7f, another gully was deposited by collapsed rocks. All the rock around the steep rock had been broken by this time. Meanwhile, a high vertical step with tens of meters of offset was found at the top of the steep rock. Thus, for the steep rock, the front was free and the back was pushed by a mass of broken rocks. These conditions along with

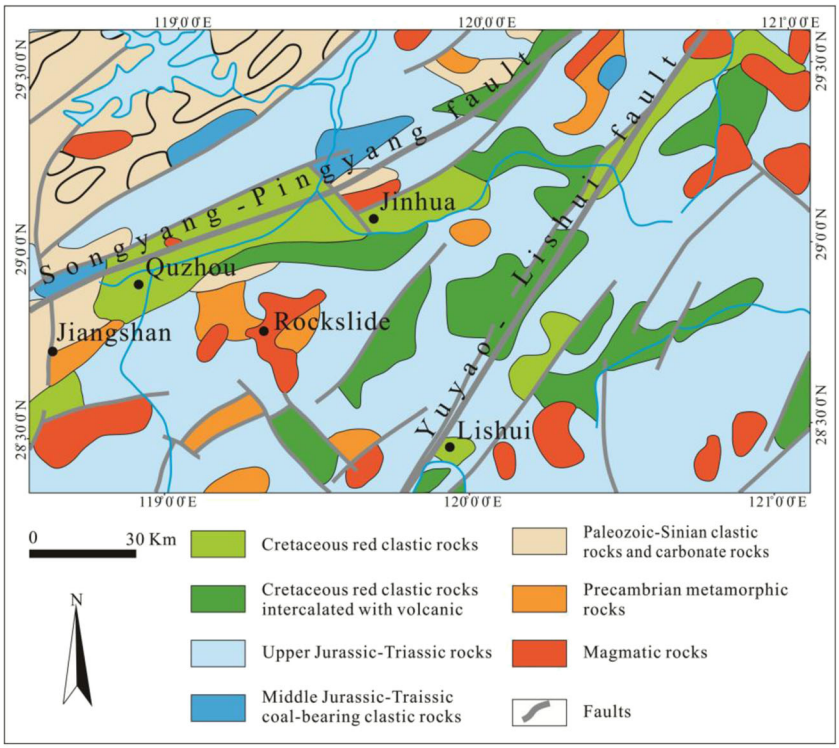

(a)

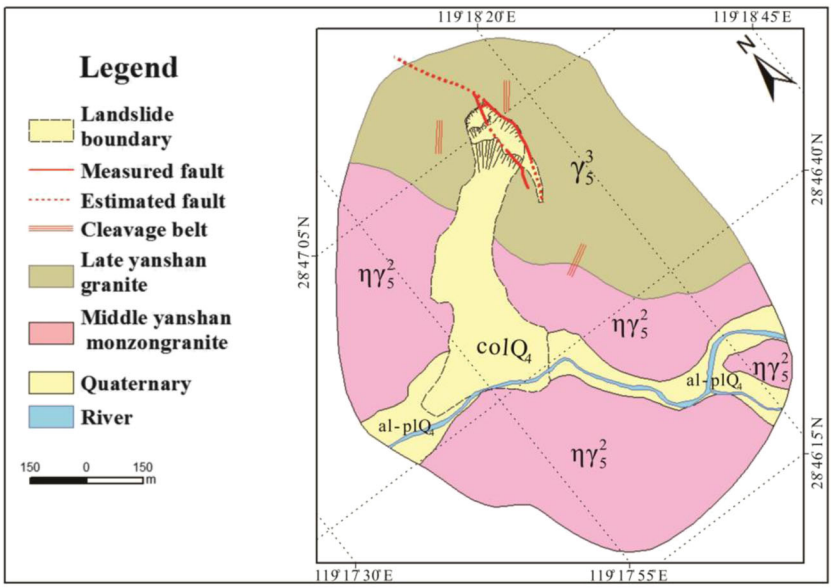

(b)

Fig. 2 Geological map of the **a** study area (modified from Ma et al. 2015) and **b** slide site

copious amounts of rainfall caused the steep rock to collapse, causing the rockslide.

Characteristics of the landslide

The initial failure area is located at the top of the mountain approximately 700 m a.s.l. From the main profile in Fig. 8a, the relative altitude difference is approximately 450 m and the runout distance is approximately 1000 m. The topographic profiles in Fig. 8a–d were created using terrain data before and after the rockslide, field data, and drilling data. The area influenced by the rockslide can be generally divided into the source area, the transition area, and the accumulation area (Fig. 3d).

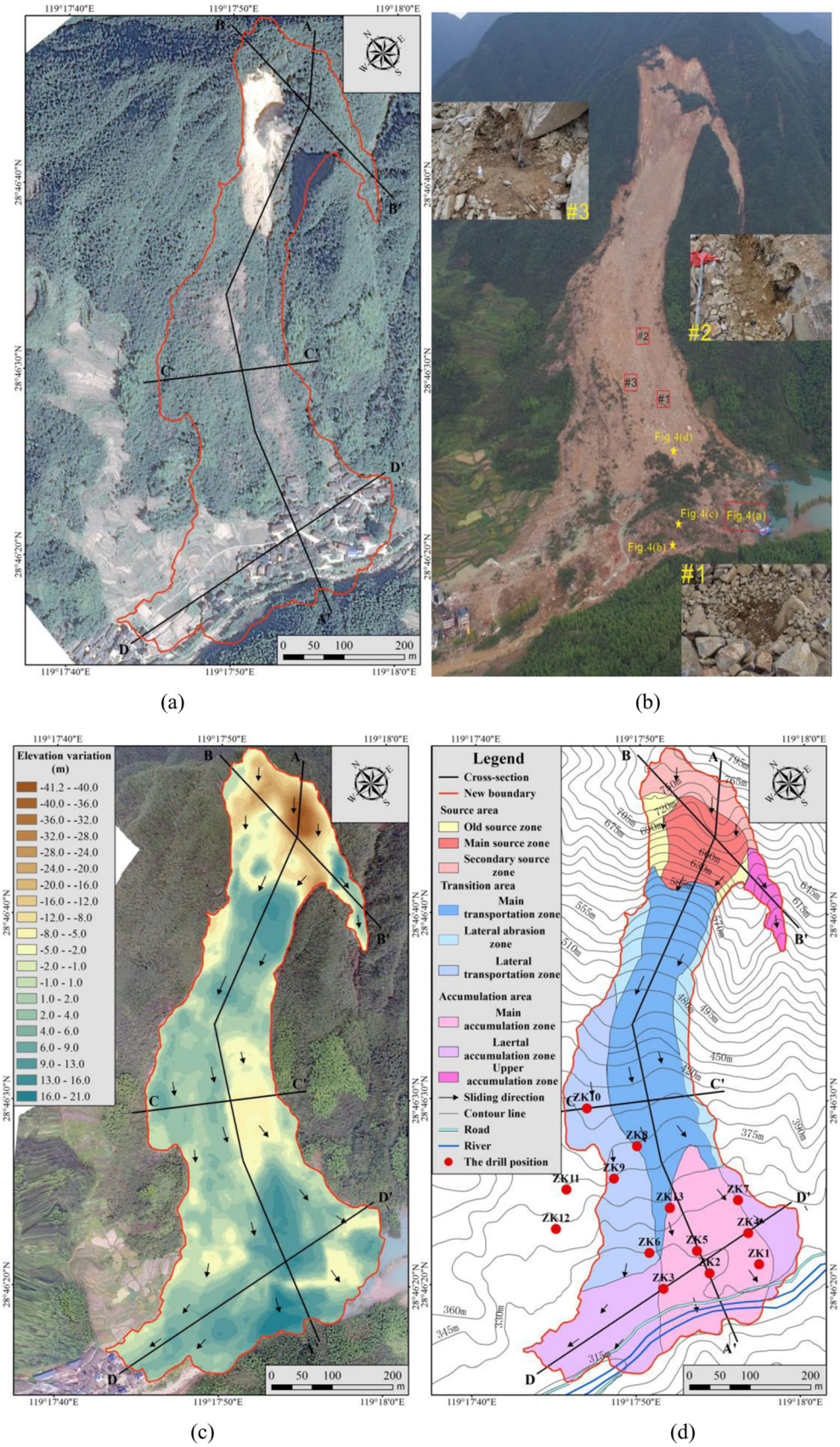

Fig. 3 **a** Quickbird image from December 13, 2013. **b** Photograph showing the study area after the rockslide (image taken by UAV on September 29, 2016). **c** The elevation variations estimated from the pre- and post-failure DEMs. **d** Topographic map and zoning of the landslide

Fig. 4 Photographs of typical rocks in the rockslide. **a** Aerial view of the deposition area. **b** Road side fence relocated by tens of meters. **c** Rocks. **d** Huge rock

Table 1 Mineral composition of the rockslide material

Mineral name	Quartz	Kaolinite	Anorthite	Albite	Muscovite	Microcline
Percentage by weight	25.8	3.1	32.6	16.5	3.7	18.3

Source area

The source area is bounded by the rear rupture, covers an area of 3.3×10^4 m^2, and has a maximum depth of 41.6 m. After the rockslide, an abrupt back with a width of 40–50 m and an angle of 52°formed. The bedrock along the failure plane is fine-grained monzogranite. In the source area, there are multiple layers of deep gray, purple, and red argillaceous fine sandstone and siltstone, which are characterized by poor mechanical properties, weathering, and structural fragmentation. According to the images and measured faults, the source area is divided into the main source zone, old source zone, and secondary source zone (Fig. 3d). The old source zone refers to the loose deposits present before the rockslide. The main source zone refers to the steep rock, which is

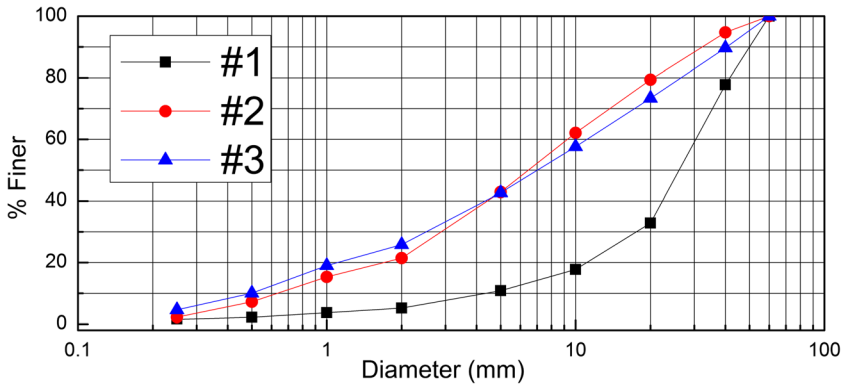

Fig. 5 Chart showing the particle size distribution of three rockslide samples

marked by the red dotted line in Fig. 7e. The mass behind the main source zone becomes unstable and moves after the steep rock collapses. The mass moved a relatively short distance and it is defined as the secondary source zone. From post-disaster UAV images in Fig. 8b, some land covered by unspoiled trees is present in the source area.

Transition area

The transition area is located in the middle of the slide and covers an approximate area of 1.05×10^5 m^3. The length of the transition area is approximately 590 m. The width of the trailing and front edges is 126 and 308 m, respectively. The transition area is mainly composed of eluvium. From the video and field investigation, the eluvium is restarted and the entrainment effect is apparent during the movement. Due to the influence of topography, the sliding direction deflected eastward about 36°. In the transition area, rocks gradually disintegrated into smaller fragments during the slide. Based on morphological characteristics, the transition area is divided into the main transition zone, lateral transportation zone, and lateral abrasion zone. The main transition zone is the fast-moving zone with the initial fragmented rocks. The large high-speed mass eroded the material along its slide. From the transverse profile C–C′ in Fig. 8c, basal entrainment is apparent and the

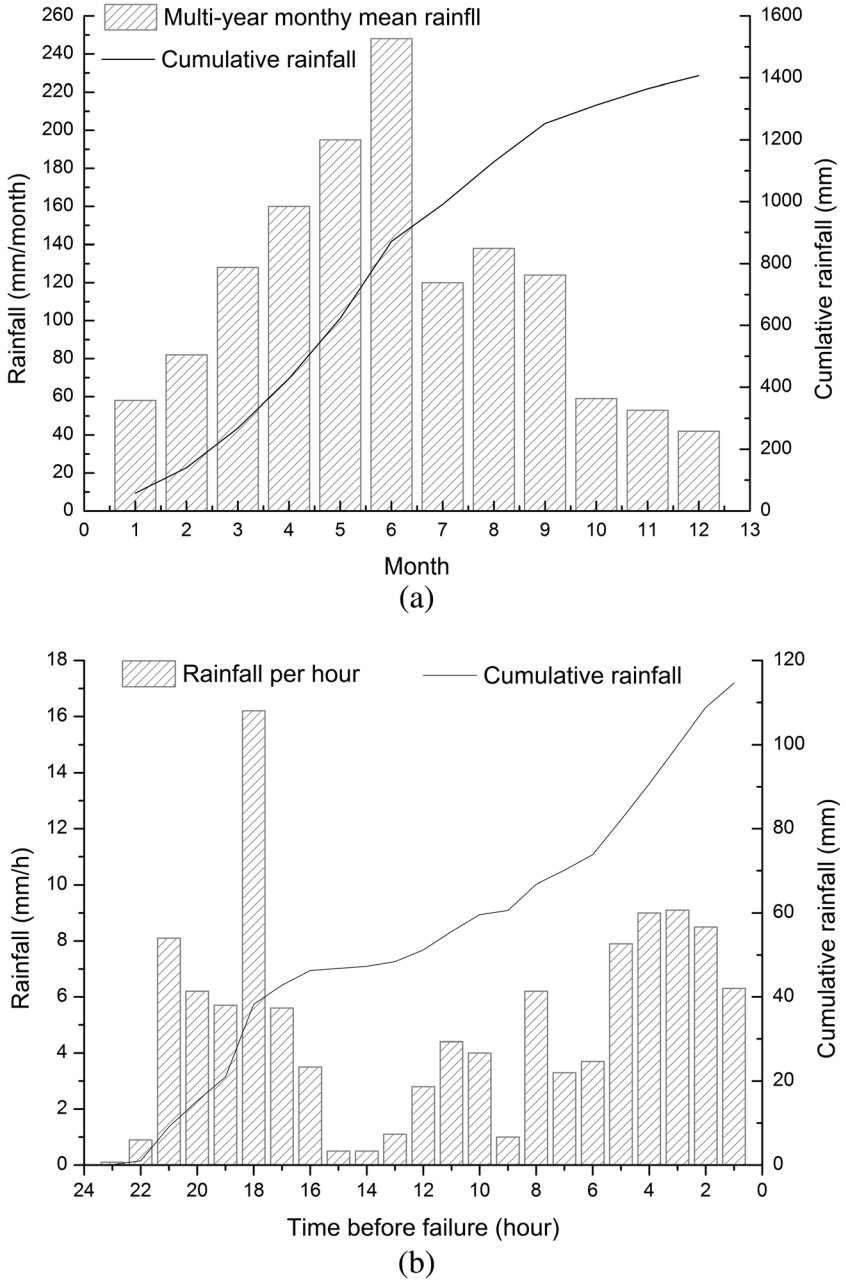

Fig. 6 **a** The average monthly precipitation data of Lishui municipality. **b** Rainfall in 1-h intervals and cumulative rainfall before the slide. Data was collected at the Wangzhaiqiao rainfall station (about 1 km away)

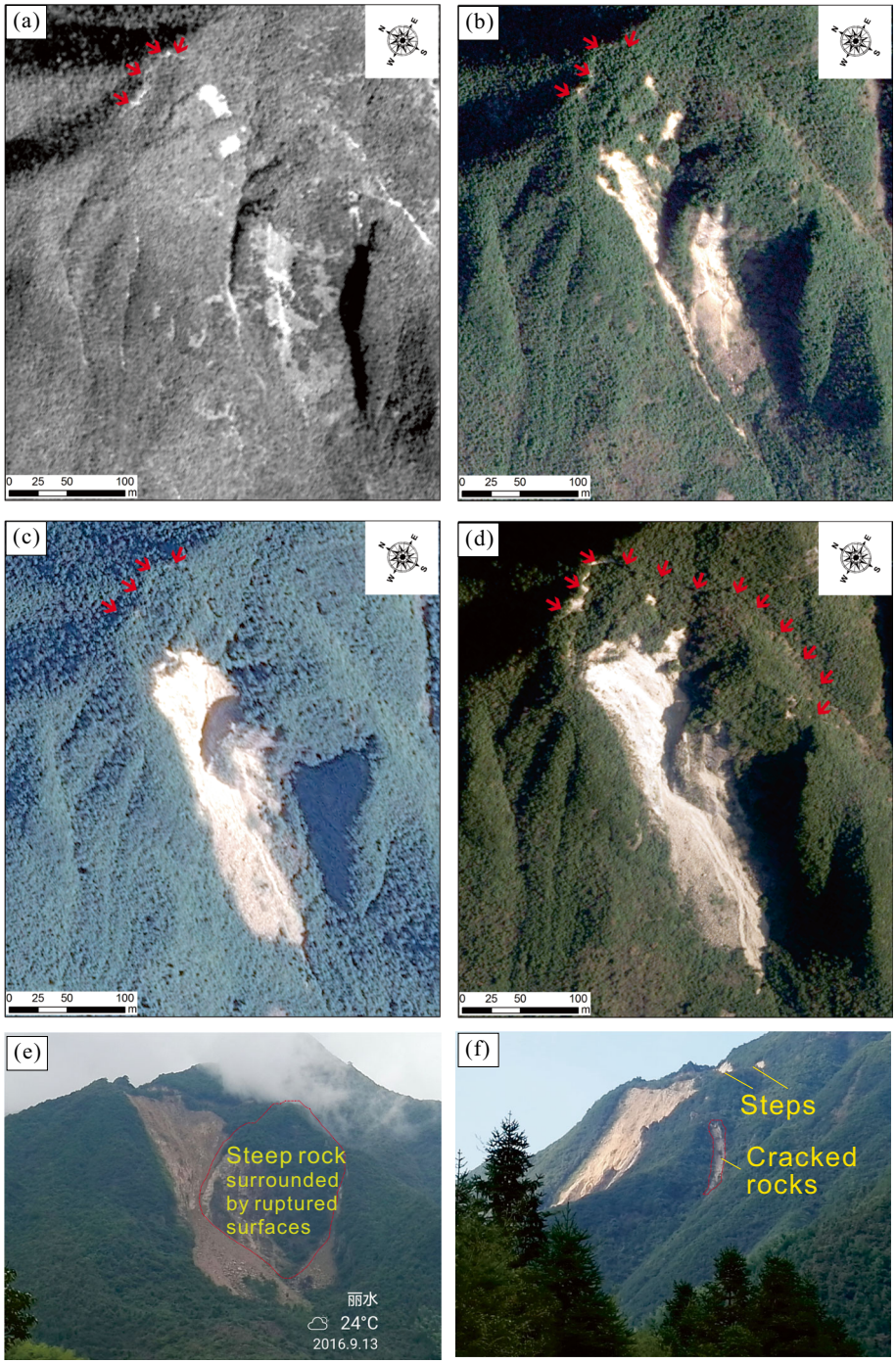

Fig. 7 Photographs of the source area for the Su village landslide. **a** KeyHole image taken in 2000. **b** Quickbird image taken in 2010. **c** Quickbird image taken in 2013. **d** Quickbird image taken in 2015. **e** Front photo taken on September 13, 2016. **f** Side photo taken on September 26, 2016

maximum depth of entrainment is about 20 m. The lateral transportation zone records a lower velocity compared to the main transition zone. In view of the drilling properties of ZK10, about 3.13 m residual soil exists, indicating the entrainment in the lateral transportation zone is apparently smaller than that in the main transition zone. Along the east edge of the main transition area, a steep slope formed. The movement consisted of primarily shallow surface abrasion, forming the lateral abrasion zone (Fig. 3d).

Accumulation area

The accumulation area covers an area of approximately 7.55×10^4 m^2 and includes the main accumulation zone, lateral accumulation zone, and upper accumulation zone. The upper accumulation zone is small and composed of rocks that moved a short distance before deposition. In the main and lateral accumulation zones, terraced fields were cultivated on the mountainside and houses and roads were built at the foot of the

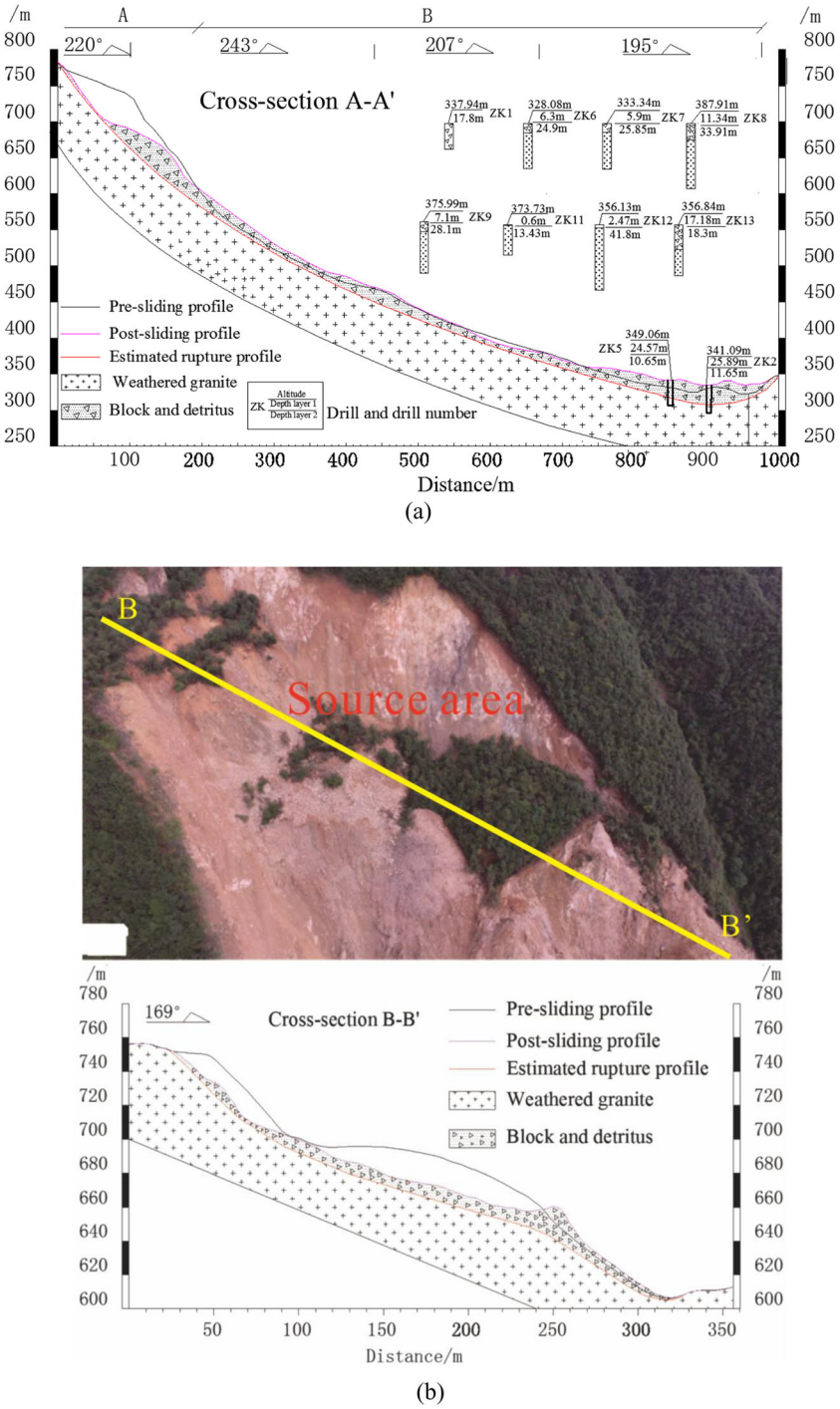

Fig. 8 Geologic cross sections along the **a** main sliding profile A–A′, **b** transverse profile B–B′, **c** transverse profile C–C′, and **d** transverse profile D–D′

mountain. Most of the rock mass was deposited in the main accumulation area. The maximum depth of the deposited mass is more than 25 m. From the transverse profile D–D′ in Fig. 8d, the area was almost covered by thick deposition in the main and lateral accumulation zones. Houses and roads in the terrace were totally wiped away due to the strong impact of the slide. The moving mass was blocked by the hill on the opposite side and was deposited in the valley.

Barrier dam and reconstruction plan

After the rockslide, a natural barrier dam and lake formed along the river. The dam mainly consisted of large rocks with a high permeability. When the water increased to the top of the dam, the water level held constant until an artificial discharge was performed. The dammed lake hampered rescue operations. Formation of the dammed lake is complicated and depends on the relationship between landslide volume, movement direction, and

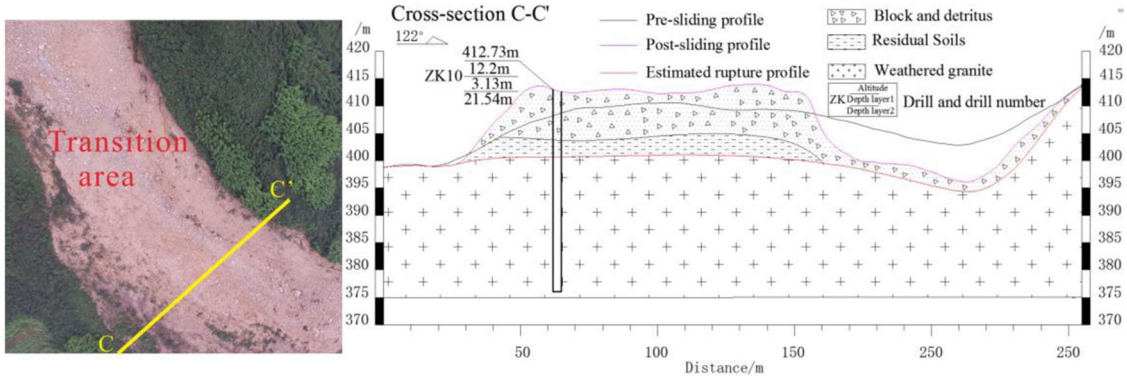

(c)

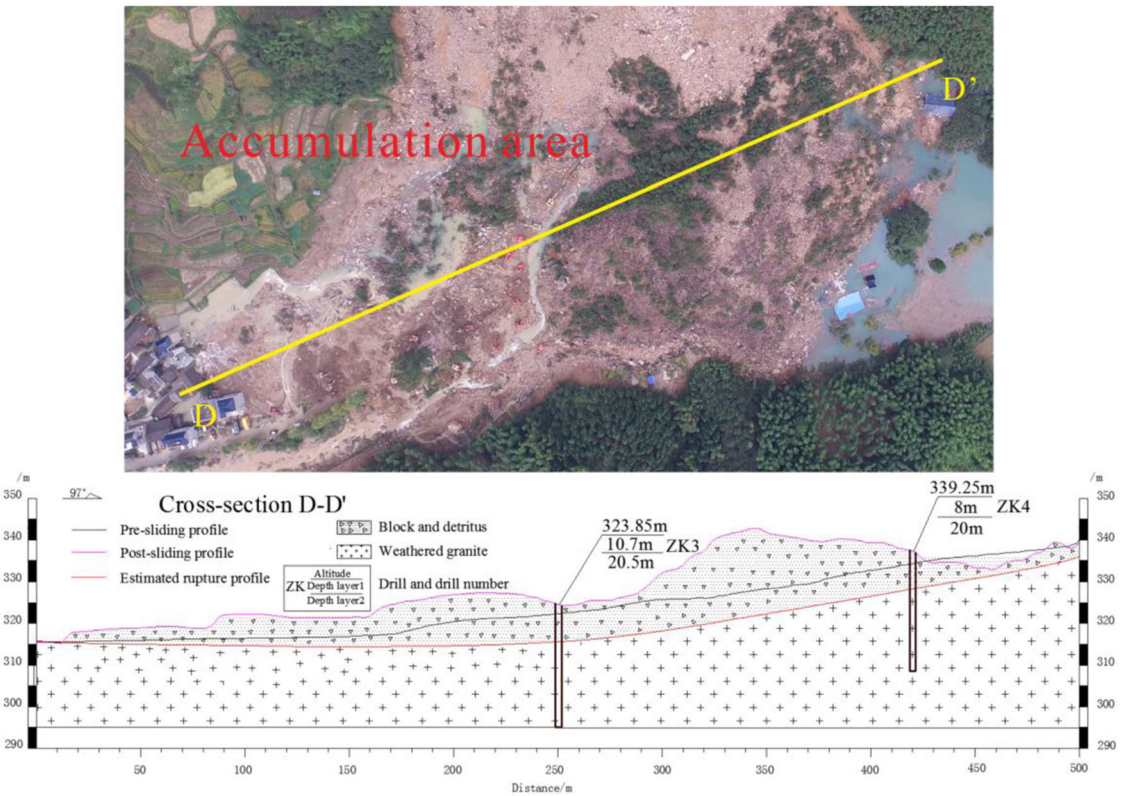

(d)

Fig. 8 (continued)

valley shape. Here, the rock mass vertically rushed into the narrow V-shaped valley. The characteristics of the barrier dam in this area are apparently different from those of Xinmo rockslide, which is another recent rockslide (Ouyang et al. 2017b; Su et al. 2017; Fan et al. 2017). For Xinmo rockslide, the valley is wide and flat, the barrier dam is low, and the lake is small.

During the rescue, the water in the lake was channeled off by digging an artificial waterway through the deposits. New multiple stable terraces were built and eco-engineering for rock slope protection was performed. The river was re-directed and the road was built on the other side of the river. The influenced area was planned to be a green space and hydrophilic park. An image of the valley after reconstruction can be seen in Fig. 9.

Concluding remarks

The Su village landslide is a typical high-elevation rocky rockslide in a mountainous area. On one hand, the potential risk from landslides is long-term and persistent in history. On the other hand, due to the limitations from scarcity of land, relocation costs and hazard awareness, numerous people live in the area. Landslides are a common problem and are becoming a major concern for mountain development and safety. Some concluding remarks are as follows:

Fig. 9 Image of the valley after reconstruction

(1) Remote sensing images can be used for preliminary evaluation of potential hazards. The potential site can be confirmed by combination of field investigation and other technical methods. After confirmation, effective evaluation of the endangered area is the key for finfinding a solution strategy.
(2) For high-elevation rocky landslides, the impact and traction force is stronger at high speeds. Thus, the basal entrainment and enlargement along the slide path are noteworthy features. These features are more apparent for old landslides or hills composed of loose deposits.
(3) For a landslide in a narrow valley, a barrier dam and dammed lake are likely to form and dramatically amplify the effect of the disaster. The formation mechanisms and stability of the barrier dam are complicated and should be considered in road planning and construction.

Acknowledgments

The abundant help from the armed police traffic team and the Department of Land and Resources of Zhejiang Province is appreciated.

Funding information This study received financial support from NSFC (Grant No. 41572303, 41520104002), CAS Key Research Program of Frontier Sciences (QYZDY-SSW-DQC006), "Light of West China" Program and Youth Innovation Promotion Association, and Funds for Creative Research Groups of China (Grant No. 41521002).

References

Chen G, Zhao Q, Huang H (2011) Sliding characteristics of high-speed and long run-out giant rockslide landslide at Wenjiagou Stream. J Eng Geol 19(3):404–408

Coe JA, Baum RL, Allstadt KE, Kochevar BF, Schmitt RG, Morgan ML, Kean JW (2016) Rock-avalanche dynamics revealed by large-scale field mapping and seismic signals at a highly mobile avalanche in the West Salt Creek valley, western Colorado. Geosphere 12(2):607–631

Cui YF, Chan D, Nouri A (2017) Coupling of solid deformation and pore pressure for undrained deformation-a discrete element method approach. Int J Numer Anal Methods Geomech 41(18):1943–1961

Evans SG (2006) Single-event landslides resulting from massive rock slope failure: characterizing their frequency and impact on society. In: Evans SG, Mugnozza GS, Strom AL, Hermanns RL (eds) Landslides from massive rock slope failure. Springer, Dordrecht, pp 53–73

Fan XM, Xu Q, Gianvito S, Dong XJ, Zhu Z, Pei XJ, Dai KR, Hans BH (2017) Failure mechanism and kinematics of the deadly June 24th 2017 Xinmo landslide, Maoxian, Sichuan, China. Landslides 14:2129–2146. https://doi.org/10.1007/s10346-017-0907-7

Guthrie RH, Evans SG, Catane SG, Zarco MAH, Saturay RM Jr (2009) The 17 February 2006 rockslide-debris avalanche at Guinsaugon Philippines: a synthesis. Bull Eng Geol Environ 68:201–213

Hu XW, Huang RQ, Shi YB, Lu XP, Zhu H, Wang XR (2009) Analysis of blocking river mechanism of Tangjiashan landslide and dam-breaking mode of its barrier dam. Chin J Rock Mech Eng 28(1):181–189

Huang RQ, Pei XJ, Cui SH (2016) Cataclastic characteristics and formation mechanism of rock mass in sliding zone of daguangbao landslide. Chin J Rock Mech Eng

Hungr O, Evans SG (2004) Entrainment of debris in rock avalanches: an analysis of a long run-out mechanism. Geol Soc Am Bull 116(9–10):1240–1252

Iverson RM, Ouyang CJ (2015) Entrainment of bed material by Earth-surface mass flows: review and reformulation of depth-integrated theory. Rev Geophys 53(1):27–58

Ma TH, Li CJ, Lu ZM, Bao QY (2015) Rainfall intensity–duration thresholds for the initiation of landslides in Zhejiang province, China. Geomorphology 245:193–206

Ouyang CJ, Zhou KQ, Xu Q, Yin JH, Peng DL, Wang DP, Li WL (2017a) Dynamic analysis and numerical modeling of the 2015 catastrophic landslide of the construction waste landfill at Guangming, Shenzhen, China. Landslides 14(2):705–718

Ouyang CJ, Zhao W, He SM, Wang DP, Zhou S, An HC, Wang ZW, Cheng DX (2017b) Numerical modeling and dynamic analysis of the 2017 Xinmo landslide in Maoxian County, China. J Mt Sci 14(9):1701–1711

Sosio R, Crosta GB, Hungr O (2008) Complete dynamic modeling calibration for the Thurwieser rock avalanche (Italian Central Alps). Eng Geol 100(1–2):11–26

Su LJ, Hu KH, Zhang WF, Wang J, Lei Y, Zhang CL, Cui P, Alessandro P, Zheng QH (2017) Characteristics and triggering mechanism of Xinmo landslide on 24 June 2017 in Sichuan, China. J Mt Sci 14(9):1689–1700. https://doi.org/10.1007/s11629-017-4609-3

Wang YF, Dong JJ, Cheng QG (2017) Velocity-dependent frictional weakening of large rock avalanche basal facies: implications for rock avalanche hypermobility? J Geophys Res Solid Earth 122(3):1648–1676

Wu JH, Chen JH, Lu CW (2013) Investigation of the Hsien-du-Shan rock avalanche caused by typhoon Morakot in 2009 at Kaohsiung county, Taiwan. Int J Rock Mech Min Sci 60(2):148–159

Xing A, Wang G, Li PB, Jiang Y, Feng PZ, Kamai T (2014) Long-runout mechanism and landsliding behavior of large catastrophic. Can Geotech J 52(7):150113073645001

Xu Q, Fan XM, Huang RQ, Yin YP, Hou SS, Dong XJ, Tang MG (2010) A catastrophic rockslide-debris flow in Wulong, Chongqing, China in 2009: background, characterization, and causes. Landslides 7:75–87

Zhen F, Yin YP, Li B, Zhang M (2012) Mechanism analysis of apparent dip landslide of Jiweishan in Wulong, Chongqing. Rock Soil Mech 33(9):2704–2712

Zhou GG, Sun QC (2013) Three-dimensional numerical study on flow regimes of dry granular flows by DEM. Powder Technol 239:115–127

Zhou GG, Cui P, Tang JB, Chen HY, Zou Q, Sun QC (2015) Experimental study on the triggering mechanisms and kinematic properties of large debris flows in Wenjia Gully. Eng Geol 194:52–61

C. Ouyang · W. Zhao · S. Zhou
Key Laboratory of Mountain Hazards and Earth Surface Process, Institute of Mountain Hazards and Environment (IMHE),
Chinese Academy of Sciences,
Chengdu, 610041, China

C. Ouyang (✉) · W. Zhao · S. Zhou
University of Chinese Academy of Sciences,
Beijing, 100049, China
Email: cjouyang@imde.ac.cn

Q. Xu · D. Peng · W. Li · D. Wang
State Key Laboratory of Geohazard Prevention and Geoenvironment Protection,
Chengdu University of Technology,
Chengdu, 610059, China

S. Hou
The Third Geological Group of Zhejiang Province,
Jinhua, 321000, China